Composites Part A xxx (xxxx) 106335

Contents lists available at ScienceDirect

Composites Part A

journal homepage: www.elsevier.com/locate/compositesa

Development of a highly efficient extrinsic and autonomous self-healing polymeric system at low and ultra-low temperatures for high-performance applications

Guillem Romero-Sabat [a], Elena Gago-Benedí [a], Joan Josep Roa Rovira [b], David González-Gálvez [a], Antonio Mateo [b], Sandra Medel [a], Ainhoa Tolentino Chivite [a]

[a] LEITAT Technological Center, Carrer Innovació 2, 08225 Terrassa, Barcelona, Spain
[b] Department of Materials Science and Metallurgical Engineering, Universitat Politècnica de Catalunya, Campus Diagonal Besòs-EEBE, Barcelona 08019, Spain

ARTICLE INFO

Keywords:
Smart materials
Particle-reinforcement
Damage tolerance
Mechanical testing
Self-healing

ABSTRACT

There is a growing demand of self-healing materials to overcome the costs derived from repairing and substituting pieces and components due continuous damages. Among the pursued strategies, the development of self-healing systems capable of operate at real low temperatures remains unsolved. In this study, we report the development of an extrinsic self-healing system for composite materials that has demonstrated an efficiency above 100% at low/ultra-low temperatures. This mechanism is based on the Ring-Opening Metathesis Polymerization (ROMP) of a blend of 5-ethylidenenorbornene/dicyclopentadiene (ENB/DCPD) monomers in the presence of ruthenium-based 3rd generation Grubbs' catalyst (G3). The blend was microencapsulated in formaldehyde-free polyurea vessels and dispersed into three different commercial epoxy resins. Tapered Double Cantilever Beam (TDCB) specimens of the modified resins were manufactured, tested and healed at low/ultra-low temperature conditions completely autonomously. All samples showed high self-healing efficiency, demonstrating the potential incorporation in real composite materials for high performance fields.

1. Introduction

Fiber reinforced plastics (FRP) are becoming more and more popular due to their improved properties allowing their use in applications that traditionally have been reserved to other compounds such as metallic and ceramic materials [1]. The main advantage of this class of composite materials is their low density, which, in combination to their mechanical properties, enable the obtention of materials that are both strong and lightweight. Weight reduction is critical in several fields, as allows an enhanced performance while providing an overall cost reduction. Thus, the lightweight materials market is growing much faster than the overall materials market [2].

With all, these materials present some undesired properties. Among those, erosion resistance due to constant loading conditions (I.e. dynamic and impact damage) is usually poor [3,4]. This erosion process can pose a severe threat to the overall integrity of the polymeric composite structure at the long pace, preventing the full inclusion of FRPs in structural pieces for its application in fields where high standards are required. Moreover, the current maintenance of FRP is posing both a technical challenge for critical structural parts as well as a great economical expense, mostly related to the fact that the possible caused damage is not always visible to the naked eye but at microscopic level [5]. In order to fully introduce those materials in some of the high-performance fields such as the automotive, wind power or aeronautic industries that will work in harsh, real conditions, there is a need for increasing the FRP on-site resistance to the erosion damage and thus, enlarging its optimum operating life in a way that not includes a higher expense in human maintenance of the materials.

Among the studied strategies used for increasing FRPs durability, service life and reliability, the development of Self-Healing (SH) materials has received a lot of attention during the last decade. By mimicking biological systems, these composite materials are designed with the ability to trigger a self-repairing response without any or with very little external human intervention when an internal or external damage is produced. Through this strategy, is possible to enhance the lifespan of these polymer composites preventing simultaneously a catastrophic failure of critical part as well as reducing significantly the maintenance of these structures. For all these reasons, SH materials are called to be

E-mail address: gromero@leitat.org (G. Romero-Sabat).

https://doi.org/10.1016/j.compositesa.2021.106335
Received 26 November 2020; Received in revised form 5 February 2021; Accepted 13 February 2021
1359-835/

the next generation of materials for high performance applications [6,7].

SH materials can be classified broadly into two types: intrinsic and extrinsic [6]. The SH process in intrinsic-type materials is due to the material's inherent characteristics and functionalities [8,9], whereas in extrinsic SH materials the damage is recovered by the release of a healing agent inside the cracks from separated microcontainers embedded in the matrix [10,11]. Although intrinsic SH materials can provide a reiterative and therefore, theoretical longer SH activity, they are in need of a relative strong external stimuli such as heat or light as well as they have lower healing volume than extrinsic systems [12–14]. In epoxy-based FRP, with some exceptions in the recent years [13,15], the main applied system is the extrinsic SH. While vasculature-like structures have been reported as SH containers, they still present scale-up and implementation problems [13,16,17], leaving the incorporation of microcapsules as the prime methodology for this approach. Overall, experimental results and literature seem to indicate that up to now, the SH approach with the highest potential of being used in real-life applications is the one based in microcapsule addition [18].

The microcapsule SH mechanism starts when the epoxy-based composite material becomes eroded and thus, micro-cracks are generated, spreading through the material. Crack propagation causes the rupture of the embedded, fragile microcapsules and the release of the healing agent that flows into the damaged area (Scheme 1, [A, B, C]). Consequently, the healing agent encounters with another embedded chemical trigger (such as a catalyst or another reactive healing agent) and polymerizes, forming a thin layer that leads to a bonding of the crack faces back together, preventing the crack propagation, delaying the erosion effect, healing the system and therefore, increasing the material's lifetime (Scheme 1, [D]).

From the wide variety of healing agents used for extrinsic SH applications (such as metathesis, polycondensation and epoxy-based systems) [16], the Ring Opening Metathesis Polymerization (ROMP) system, on which this work is based upon, has been extensively reported in the literature and it has proven to be an excellent polymerization technique for these SH thermoset materials. Studied first by White *et al.,* the ROMP of blends of cyclic olefins is used to synthesize linear and ramified polymers through the action of ruthenium-based catalyst (Grubbs', Hoveyda-Grubbs') [19]. These catalysts can be either directly dispersed into the resin or encapsulated in waxy materials in order to avoid a deactivation by contact with the curing agent or exposure to air [20]. Even though there is a broad number of SH studies reporting the use of Grubbs catalyst, to the best of our knowledge this is the first work reporting the use of the 3rd generation of Grubbs catalyst, with a reactivity that can be up to six orders of magnitude higher than 2nd generation [21], for SH applications.

5-Ethyldiene-2-norbornene (ENB) and dicyclopentadiene (DCPD) mixtures, (ENB/DCPD) microencapsulation has been reported using *in-situ* polymerization in urea-formaldehyde [22,23] and melamine-urea-formaldehyde [24]. However, problems regarding the use of solvents or toxic formaldehyde, represent a drawback in the use of those materials. Above them, polyurea (PU) rises as a good alternative as it is stable at

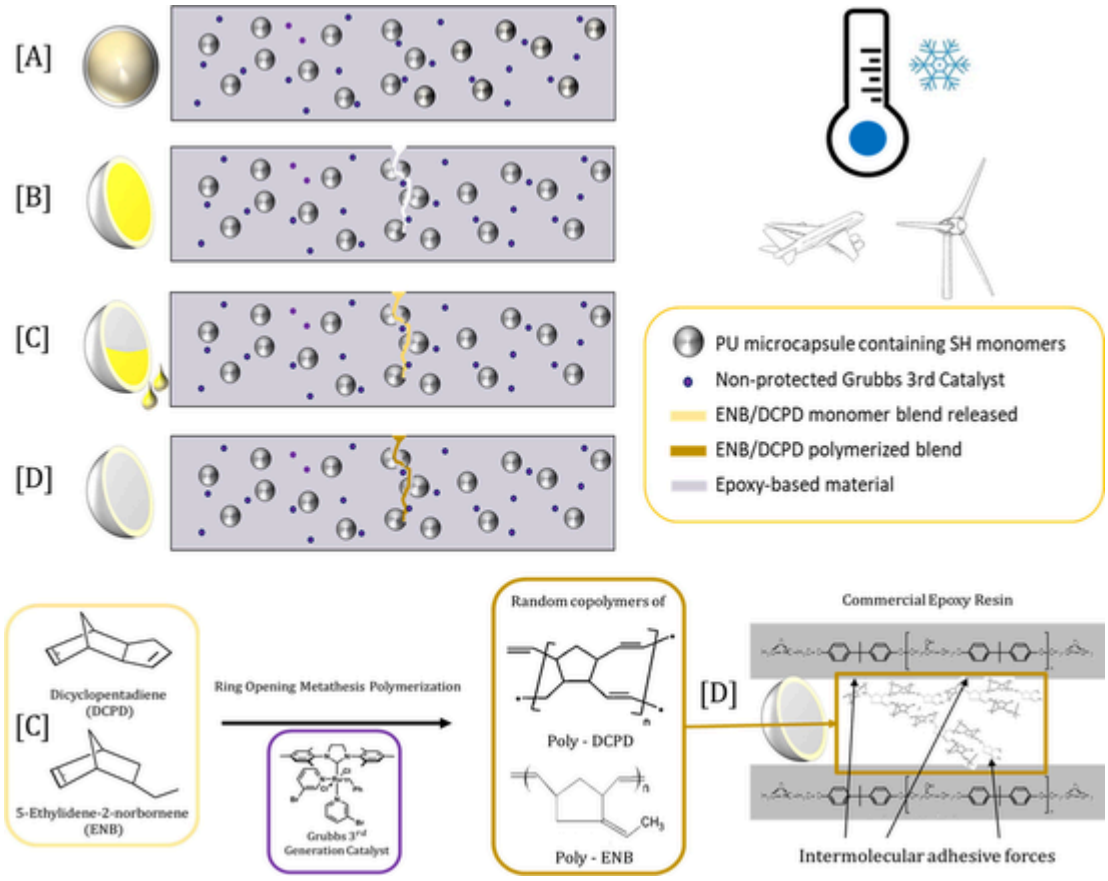

Scheme 1. Scheme of the extrinsic ROMP-based self-healing system developed in this work for epoxy-based materials used in high demanding fields efficient at ultra-low temperatures. The self-healing mechanism reported in this work follows the same ROMP-based chemistry as previous bibliography [10,12,19,26]. In short, strained cyclic olefins with no bulky groups around the double bonds such as 5-Ethylidiene-2-norbornene (ENB) and Dicyclopentadiene (DCPD) are microencapsulated and dispersed in epoxy-based materials. When a crack appears (due to erosion or external damage, for example), it breaks the composite along with the capsules, the monomers are released from their vessels and reacts at low temperature (−20 °C) in presence of a Ru-based catalyst (3rd Generation Grubbs Catalyst) previously embedded into the material to generate a crosslinked random copolymer of poly-ENB/DCPD, generating an adhesive layer and attaching both sides of the damaged composite. With this, the material is healed and its operating shelf-life, increased.

the different processing conditions—it has been used for other self-healing systems—[25], and the methodology is formaldehyde and solvent-free. The main problem may be envisaged from the use of isocyanates for the polyurea formation, but the risks are minimized by using non-volatile polyisocyanates and by assuring non-free isocyanates in the final product (using amine excess and following isocyanate consumption by FTIR).

Furthermore, current microcapsule-based SH materials have good performance under favourable and standard conditions, but have failed to provide a good repairing performance at harsh conditions, especially, at very low temperatures where the real operation conditions of the materials used in aerospace or windmill industry take place. In the last years, some ROMP-based systems with potential to operate at sub-zero temperatures have been demonstrated and microencapsulated, but the self-healing tests were only performed at room temperature and low yields were obtained [26]. Alternatively, Kalista and coworkers reported a system able to work at low temperatures but with the need of external sources of energy (ballistic impacts) to initiate the self-healing process [27]. Dong-Min, et al. demonstrated a successful dual microcapsule low temperature (−20 °C) self-healing, but for coating applications [14]. Regarding intrinsic self-healing systems, several works mention a development of a self-healing system operating at low temperature while really they refer to room temperature or near ambient temperature [28,29]. Only a few works such as the ones from Wu et al. or Xue et al. show a successful, real self-healing behaviour at low temperature [30,31] and, in none of them, the selected matrix is either a thermoset or epoxy-based. The failure of intrinsic systems for low temperature applications may be hypothesized to be related to the need of a significant chain mobility to achieve the regeneration process [12,32]. Thus, all of these systems fail to provide an effective extrinsic-type and autonomous (understood as the unnecessity of needing any external agent, such as heat, pressure or radiation) [12] SH solution for internal structural components for the real environmental conditions that the materials will face.

Hence, in this study the authors report the development of i) an extrinsic self-healing system based on metathesis polymerization of ENB/DCPD blend, able to flow without phase separation at −70 °C and to react, in presence of 3rd generation Grubbs' catalyst from −20 °C; ii) ENB/DCPD blend microencapsulation by interfacial polymerization in solvent-free non-toxic polyurea (PU) generating core-shell microcapsules with up to 70 wt% load; iii) the incorporation of these microcapsules into different system of epoxy-based material without the necessity of protecting the metathesis catalyst; and iv) the demonstration that this system present an autonomous healing efficiency in fracture toughness assay with tapered double cantilever beam (TDCB) [33] higher than 100%, at cryogenic temperatures for all different epoxy systems.

2. Experimental section

2.1. Materials

Three different epoxy systems (Table 1) were used as polymeric matrixes for the specimen's manufacture. Grubbs 3rd generation (G3) and Hoveyda-Grubbs 2nd generation (HG2) catalysts were purchased from Sigma-Aldrich. 5-Ethyldiene-2-norbornene (ENB) and dicyclopentadiene (DCPD) were used as healing agents and purchased from Sigma-Aldrich (US). Voranate™ M 2940 (Dow, US) was used as polymeric isocyanate (polymeric methylene diphenyl diisocyanate pMDI). Ethylendiamine (EDA), Diethylenetriamine (DETA) tetraethylenetriamine (TETA) and arabic gum from acacia tree were purchased from Sigma-Aldrich and used as received.

Table 1
Curing conditions of the different epoxy resin systems.

Resin system curing rate			Parts per weight	Curing process
Epoxy component	Amine curing agent	Accelerator		
Epikote RIMR 135	Epikure RIMH 137	–	100 : 35	Ramp at 0.5 °C/minute to 45 °C. Hold at 45 °C for 1 h. Ramp at 1 °C/min to 75 °C. Hold at 75 °C for 4 hrs. Cool to ambient at 1 °C/min. Hold at RT for 19 h. No post-cure process is performed
Araldite LY 556	Aradur HY 917	DY 070	100 : 90: 0.5–2	Ramp at 1 °C to 65 °C. Hodt at 65 °C for 1 h. Rampt at 1 °C/min to 80 °C. Hold at 80 °C for 16 h. Cool to RT at 1 °C/min. No post-cure cycle is performed
CTD 7.1 Part A	CTD 7.1 Part B	–	101 : 29.6	The sample is cured for 7 days at 25 °C. No post-cure process is performed

2.2. Sample preparation

2.2.1. ROMP monomers selection

At low temperatures, fast reaction kinetics are beneficial for the self-healing process. Therefore, strained cyclic olefins having no bulky groups around the double bonds, such as 5-ethylidene-2-norbornene (ENB) and dicyclopentadiene (DCPD), were selected due to their extensively reported high ROMP activity [34]. The ENB monomer has a higher ROMP reactivity than DCPD, however; DCPD is a good candidate since it provides enhanced mechanical properties to the final polymer such as fracture toughness and strength, which are achieved due to the cross-linked structure obtained after polymerization [23].

Nevertheless, the melting point of DCPD (32.5 °C) limits its use as monomer as it is waxy at 20 °C and solid at sub-zero temperatures therefore, it cannot flow and fill the cracks. On the contrary, mixtures of ENB and DCPD present much lower melting points. It has been reported that mixtures of ENB/DCPD in a ratio of 95:5 are suitable to be used as liquid healing agent as low as −50 °C [26].

Solubility and phase separation of the different ENB/DCPD blends were studied by mixing each monomer at its specific ratio in a vial and kept at room temperature, −20 °C and −70 °C from 1 h to several days. The blends were visually observed periodically to determine possible phase separation. Moreover, their viscosity was quantified at the selected temperatures to demonstrate the blend's fluidity.

2.2.2. Catalyst selection

Ru-based catalysts, such as those from the Grubbs' family, are reported as ROMP reaction catalysts in SH systems [34,35]. Since fast-initiating catalysts are necessary to promote metathesis at reduced temperatures according to our application [36], two different Ru-based catalysts with low activation temperatures were selected [36]: Hoveyda Grubbs 2nd Generation (HG2), and Grubbs 3rd Generation Catalyst (G3).

Reactivity of the different ring-opening metathesis catalysts (HG2 & G3) was verified in the first place visually and by FTIR through the formation of crosslinked networks of the polymer. Each catalyst (C = 0.1 wt% to 0.004 wt%) and ENB/DCPD (95:5 and 80:20 molar ratio) were mechanically mixed in a previously cooled vial (−72 °C) and kept at room temperature, −20 and −70 °C for up to 10 days. The maximum time the sample remained under study was 14 days. After the first qualitative screening, catalyst activity and reactivity were quantified by DSC through the assessment of the heat released from the

exothermal ROMP reaction. To ensure that no reaction took place prior to the measurement, the blends were mixed with the selected catalyst at −72 °C and approximately, samples of 5 mg of the mixtures were added to a cooled aluminium pan, hermetically closed and allowed to rest for 10 min prior to perform a heating ramp at 5 °C/min. In these experimental assays, the influence of the concentration of the catalyst of each kind was studied as a mean to determine the minimal quantity at such temperatures.

2.2.3. Procedure of ROMP monomers microencapsulation

ENB/DCPD microcapsules were prepared via interfacial polymerization. Initially, an oil-in-water emulsion was prepared by slow addition of the oil phase, composed of the healing agent (ENB/DCPD 80:20 wt%) and the isocyanate (pMDI, quantity depending on the core/shell ratio), over 3.5 wt% gum arabic aqueous solution and the mixture was stirred (2500–5000 rpm) in a homogenizer (Dispermat CV3-Plus with Homogenizer SR 03-01, VMA-Getzmann GMBH, Germany) for 20 min.

Later, the emulsion was transferred to a jacketed reactor, stirred at 400 rpm and EDA or TETA (1–5% aqueous solution, 1.1–1.5 eq) was added dropwise from a pressure compensated funnel. After the addition was completed, the temperature was increased and the mixture was stirred until a complete reaction of the pMDI with the amine occurs.

The resulting milky dispersion was filtered under vacuum (2 μm, Nylon) and washed with water twice. Finally, the cake was dried at 30 °C under vacuum to render a raw white solid.

2.2.4. Microcapsules dispersion in epoxy resins and tappered double cantilever beam (TDCB) specimens preparation

The unfilled, neat specimens were manufactured by carefully mixing the different components of each resin system on the specified proportions as stablished by the manufacturer (Table 1). For the synthesis of the SH specimens, a dispersion process based on previous bibliography was performed [37]. First, a specified amount of SH microcapsules (0–30 wt%) and ruthenium-based catalyst (0.004–0.1 wt% respect monomer weight) were added into the epoxy component of the resin. Next, the mixture was mechanically stirred at 500 rpm using a Dispermat CV3 (VMA-Getzmann GMBH, Germany) at room temperature for 15 min. Then, the remaining resin components were added, followed by 5 min mixing at 800 rpm.

The mix was poured finallyinto a silicon mould with the TDCB geometry defined in previous works [38], and cured in a staged protocol recommended by the manufacturer for a full cure process (Table 1). The additive containing self-healing resins were cured following the same procedure as the neat ones.

2.3. Characterization methods

2.3.1. Particle size

The average particle size and particle size distribution of the microcapsules were measured by laser diffraction using a Mastersizer 3000 (MAZ3000, 0.1–1000 μm range, Malvern Panalytical, UK).

2.3.2. Thermogravimetric analysis (TGA)

TGA was carried out with a Q500 thermobalance (TA Instruments, US). Resin samples were heated from 25 °C to 1000 °C at a 10 °C/min heating rate under air and nitrogen flow. The weight loss was recorded as a function of temperature.

2.3.3. Differential scanning calorimetry (DSC)

The DSC was cooled to −75 °C and then, a cooled sample of approximately 5 mg was introduced ensuring the temperature did not surpass −70 °C. Each sample was heated in a ramp of 5 °C/min from −65 °C to 150 °C and the onset temperature (T_{onset}) as well as the peak temperature (T_p) were recorded. Due to the system's high exothermic polymerization reaction, the T_{onset} of the system is used as reference to point the starting temperature of the self-healing.

2.3.4. Fourier transform infrared-attenuated total reflectance (FTIR-ATR)

The infrared spectra were obtained by using an IR Affinity-1S CE FTIR spectrophotometer (Shimadzu, Japan) in the 4000–500 cm^{-1} range and with a 1 cm^{-1} resolution (32 scans collected).

2.3.5. Microcapsules and composites morphology

Scanning Electron Microscope (SEM) micrographs were obtained with a SEM Touchscope JEOL JSM-6010LV (JEOL instruments, Japan) and a Phenom XL Desktop SEM at acceleration voltages of 5 kV. Prior to the SEM observation, the specimens were coated with a thin conductive layer by using a sputter coater (Cressington scientific instruments, 108 Auto).

For the characterization of inner part of microcapsules, thin slices of microcapsules embedded in Epikote:Epicure epoxy resin (see Section 2.4) are produced by using a RM2255 manual rotary microtome (Leica Biosystems, Germany).

After curing, the homogeneity of the microcapsules dispersion into the cured resin and their integrity were evaluated by SEM (Touchscope JEOL JSM-6010LV, JEOL, Japan). Thin slices of the material (40 μm thick) were obtained by Microtome (Leica MR 2255) and further metallized with Au.

2.3.6. Focused ion beam (FIB)

Internal microstructure for the different tested specimens was characterized by micro-machining cross-sections at the central part of the different microspheres by means of focused ion beam (FIB). Cross-sectioning and the subsequent field emission scanning electron microscopy (FESEM) observations were conducted using a dual beam workstation (Zeiss Neon 40). A thin platinum layer was deposited on the region of interest prior to FIB with the main aim of reducing ion-beam damage. Then, a Ga^+ ion source was used to mill the surface at a voltage of 30 kV. A final polishing of the cross-section was performed at a current of 500 pA in order to get more details related to microstructure of the different microspheres investigated in the present study.

2.3.7. Nuclear magnetic resonance (NMR)

^1H NMR spectra are acquired in a Bruker Avance-II + 600 MHz (14T). NMR spectra of the self-healing loaded microcapsules were obtained in Deuterated Dichloromethane (DCM-d_2) and compared to the NMR spectra of extracted self-healing mixture after microcapsules swelling in acetone-d_6 and filtration through 0.45 μm pore nylon filters.

2.3.8. Viscosity of monomeric blends

The behaviour of the monomeric blends at different temperatures was quantified by measuring the elucidation time in a Ford 3 cup previously cooled at the selected temperature (−70, −20 °C, room temperature). For reference, a parallel measurement at 20 °C between the same monomer blend in the viscosity cup and in the Bohlin Gemini rheometer (Malvern Panalytical, UK) using a cone-plate geometry and a shear rate from 0 to 83 s^{-1} were performed.

2.3.9. Rheological behaviour of uncured epoxy resins

Instantaneous viscosities of the neat resins and the microcapsules loaded resins were determined at 25 °C under a shear rate from 0 to 83 s^{-1} using a parallel plate geometry in a Bohlin Gemini rheometer (Malvern Panalytical, UK).

2.3.10. Self-healing testing

As a mean to evaluate the self-healing performance and efficiency, a modified method based on the previously stablished by White *et al.* has been followed [19]. Shortly, the specimen was placed in an ultra-

freezer at −80 °C for 48 h to ensure a homogeneous ultra-low temperature. Afterwards, in order to assure the correct direction of the propagation of the breaking line, a notch was made into the specimen using a sharp razor blade.

The cold specimen was loaded in the instrument and the tension-displacement test started while controlling the load in order to stop the experiment when a drop of force during the assay is detected. The temperature was registered during the assay using an infrared thermometer IAN 291541 (Powerfix Profi, Germany). Immediately after the test, the specimen was placed in a chest freezer of ultralow temperature (EHF, 78/86 from Equitec, Spain) and allowed to heal keeping cryogenic conditions (−20 °C) for 48 h. After the healing time, the sample is cooled to −80 °C to ensure it remains cold during the assay and the test is performed again.

The overall duration of the measure, from the moment the specimen was removed from the ultrafreezer until it was placed again did not exceed 6 min and the specimen temperature did not achieve temperatures above −20 °C.

The specimens were tested by using the Instron 1341 machine working under loading control mode. The tests were conducted under displacement mode at a constant deformation speed of 5 $\mu m \cdot s^{-1}$, which, carefully developed by previous investigations [19] helps to control the crack growth along the centre line of the brittle specimen.

The fracture healing efficiency in the case of quasi-static fracture conditions (η), can be calculated by using the following equation provided by previous studies [19,39]:

$$\eta\,(\%) = \frac{K_{c\ healed}}{K_{c\ virgin}} * 100 \quad (1)$$

Equation (1). Self-healing efficiency equation for quasi-static fracture conditions.

Where η is defined as the ability of a healed sample to recover fracture toughness, Kc_{virgin} is the fracture toughness of the virgin specimen and Kc_{healed} is the fracture toughness of the healed specimen.

Typically, in order to calculate the sample toughness, it would be necessary to integrate the equation obtained from the load-displacement curve. However due to the specific geometry of the TDCB specimen, the sample toughness is equal to the critical load (Pc) multiplied by a geometrical constant (α), thus giving: $K_c = \alpha * P_c$; that can be simplified, [40] therefore, reducing the equation to the following:

$$\eta\,(\%) = \frac{P_{c\ healed}}{P_{c\ virgin}} * 100$$

Equation 2. Simplified self-healing efficiency equation for quasi-static fracture conditions. Due to the TDCB geometry, the fracture toughness (Kc) can be substituted by the critical load (Pc) [40].

Pc, the critical load, is defined either as the point where the TDCB specimen breaks or the point in the load (N) vs displacement (d) curve where the load drops, meaning that the tensile test starts to propagate the crack generated by the razor blade. Moreover, surface morphology of the cured virgin and healed TDCB specimens were carefully studied by SEM to observe the possible differences in the microcapsule structure.

3. Results and discussion

3.1. Fluidity and reactivity at different temperatures

The liquidity of the ENB/DCPD mixtures were studied at 1, 4, 24 and 72 h. Neither phase separation nor appearance of solids was found at −70 and at −20 °C in monomer mixtures from 100:0 to 80:20 ENB/DCPD ratios. Although there was a proportional increment of the quantified values of viscosity as the temperature lowered and the ratio of DCPD monomer was increased (Fig. 1), the maximum efflux time obtained was 16.6 s for the 80:20 blend at −70 °C, only 3.7 s above the liquid reference of 100:0 ENB, thus supporting the fluid behaviour observed at all studied temperatures and blends. For further research in this study, ratios of 95:5 and 80:20 were selected as, based on literature, [41] they were respectively the mixtures with higher reactivity and with more crosslinking capacity.

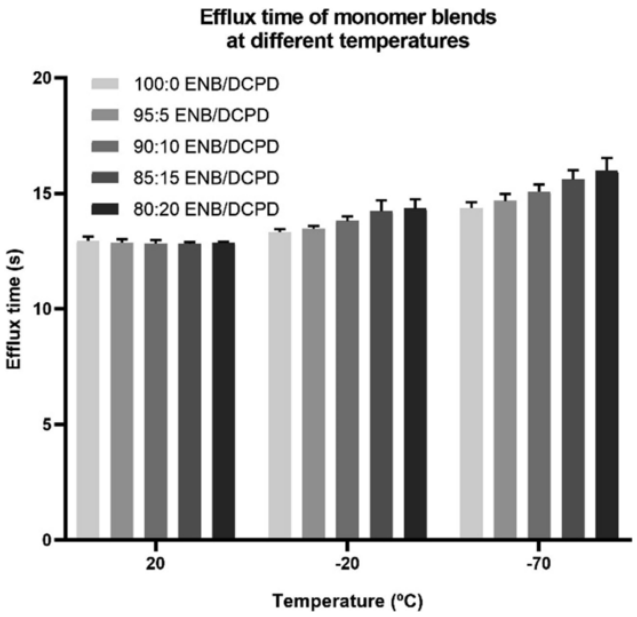

Fig. 1. Graph showing the efflux time of the different monomer blends at different temperatures with a Ford #3 Cup. Pure ENB (100:0) was used as reference as the solidification temperature of ENB is set at −80 °C. Although at room temperature no difference was observed in the Efflux time, which is related to the material's viscosity, between the different blends, there is an observable increase when either the temperature is lowered or the ratio of DCPD monomer is increased, leading to the highest value at −70 °C and 80:20 ENB/DCPD. However, the time only increased for approximately 3 s, demonstrating thus the fluidity of the blends even at ultra-low temperatures. No appearance of solids was observed in any blend at any temperature.

A first qualitative comparative assay between catalysts at different concentrations proved G3 to be the most active catalyst for the selected ENB/DCPD blends both at room temperature and at −20 °C, in coherence with previous reported data [42].

At −70 °C there was no evidence of reaction of any blend with any catalyst concentration

As a mean of obtaining quantifiable values for the reactivity of the catalysts at low temperature, blends of ENB/DCPD were produced againand mixed respectively with a high concentration of 0.1 wt% of the selected catalysts (Table 2). HG2 exhibited both the T_{onset} and the T_p at higher temperatures than those of G3. Moreover, a proportional reactivity pattern (lower T_{onset}) could be envisioned when a higher load of ENB was used. Over time, HG2 and G3 have been shown similar yields but G3 is a considerably better catalyst at low-T, presumably because dissociation of the electron-deficient 3-bromopyridine ligand is

Table 2
Summary of the T_{onset} and T_p of the different ENB/DCPD blends with 0.1 wt% of HG2 and G3 catalyst.

	ENB/DCPD (wt.%)	T_{onset} (°C)	T_p (°C)
Hoveyda-Grubb's 2nd Catalyst at 0.1 wt%	95:5	0.84	18.04
	80:20	1.90	17.91
Grubb's 3rd Catalyst at 0.1 wt%	95:5	–22.66	2.36
	80:20	–18.94	4.42

extremely rapid and/or because rebinding is slow, both of which contribute to favorable turnover conditions [43]. Acknowledging thus the lower reactivity of HG2 vs G3 for low temperature applications, HG2 was discarded from further work in this study.

In order to determine the optimal concentration of G3 catalyst for the SH systems, reactivity of 0.01 and 0.004 wt% with different blends were produced and measured with DSC (Table 3).

The obtained results with the monomer reactivity are in coherence with all the data previously observed (Table 2) as well as the collected by other researchers [26,42]. First, it is observable that due to the DCPD's lower reactivity compared with the ENB monomer, the increase of DCPD content in the blend causes a decrease in both the T_{onset} as well as on the T_p. Moreover, the increment of catalyst shows evidence of lowering the activation temperature several degrees as assessed in the previous qualitative experiments.

Nonetheless, all the selected ratios at the chosen G3 catalyst concentration confirmed a good cryogenic reactivity and therefore, have potential to be used as a self-healing reactivity blend for the intended application.

With all the collected data, the selected system for the encapsulation was ENB/DCPD 80:20 ratio monomer mixture with 0.01% G3 catalyst. This selection was considered a compromise between: i) suitable fluidity at both –20 °C and –70 °C as well as good polymerization times at –20 °C, ii) the more crosslinked final polymers with theoretical mechanical improvement provided by higher contents of DCPD and iii) the economic cost of the last generation Grubbs catalyst.

3.2. Microcapsules synthesis

Interfacial polymerization methodology allows obtaining a wide range of microcapsules as there are several variables to play with: polyisocyanate and polyamine used, isocyanate/amine ratio, core/shell materials ratio, water/oil phase ratio in the emulsification step, emulsifier (type and amount), polyamine dilution, reaction temperature and stirring rate (both emulsification and polymerization steps). In addition, the microcapsules requirements were defined: minimum quantity of free isocyanate, <20 μm diameter, minimum release produced by porosity, maximum core/shell ratio and high temperature resistance (more than 200 °C).

Table 3
Summary of the T_{onset} and T_p of the different ENB/DCPD blends with 0.01 wt% and 0.004 wt% of G3 catalyst. Graphs and results of all other blends can be observed in the Suporting information.

	ENB/DCPD (wt.%)	T_{onset} (°C)	T_p (°C)
Grubb's 3rd Catalyst at 0.01 wt%	95:5	–22.54	2.69
	80:20	–18.32	4.45
Grubb's 3rd Catalyst at 0.004 wt%	95:5	–18.76	3.76
	80:20	–17.30	4.81

First, the conditions of ENB/DCPD emulsion in water step were optimized an fixed as 70:30 water/oil ratio and 3–3.5% of Arabic Gum as emulsifier [44].

In the encapsulation method developed, the oil phase is composed of END/DCPD (80:20 weight ratio), as previously stated, mixed with a low viscosity pMDI (Voranate™ M2940). Once the emulsion is formed, a diluted aqueous solution of the polyamine is added to react with pMDI and form the polyurea wall of the microcapsules (Fig. 2) [44].

The effect of the variables of emulsion (stirring rate) and polymerization (amine type and concentration, reaction conditions) steps in the morphology, shell polymer conversion and thermal resistance of microcapsules have been studied and compared. This was investigated with the aim of obtaining robust and stable core-shell microcapsules with the maximum loading of healing core and with the highest thermal resistance for the production of composites. Reaction conditions and properties of the obtained microcapsules (MC1-MC19) are gathered in Table 4 and their SEM images in Fig. 3. First short alkyl chain polyamines were used (EDA, DETA and TETA) in order to minimize the ENB/DCPD release due to wall porosity (MC1-MC3). Only EDA rendered small individual spherical microcapsules, as DETA and TETA lead to coagulation (Fig. 3a).

When comparing the morphology of microcapsules with different core/shell ratios and fixed amine concentrations (1% aqueous solution added at a 1.1 ratio to isocyanates), MC1, MC4 and MC5 it was observed that a spherical morphology was obtained at all the studied ratios: 60:40, 70:30, and 80:20 (Fig. 3- a, c and d). Within this context, if both core/shell ratio and amine concentration were increased above 80:20 and up to 4% respectively to accelerate the reaction (MC12 and MC13), the microcapsules became slightly deformed in one axis presenting an elongated shape (Fig. 3- j and k). This effect may be associated to insufficient material for wall forming and so particle merging. It is worth mentioning that 70:30 core:shell ratio MCs lead to closest contents of healing agents to theoretical value (70%) of the studied samples, resulting in most efficient encapsulation system. In addition, the rendered materials of 70:30 core:shell proportion showed higher degradation temperature (250 °C) when compared to other ratios.

On the other hand, the aforementioned systems present an incomplete isocyanate consumption during the chemical reaction as shown in the FTIR spectra by means of presence of NCO peak corresponding to the signal at 2272 cm^{-1}. In order to improve isocyanate reaction, the effect of both the equivalents of amine and its concentration in the

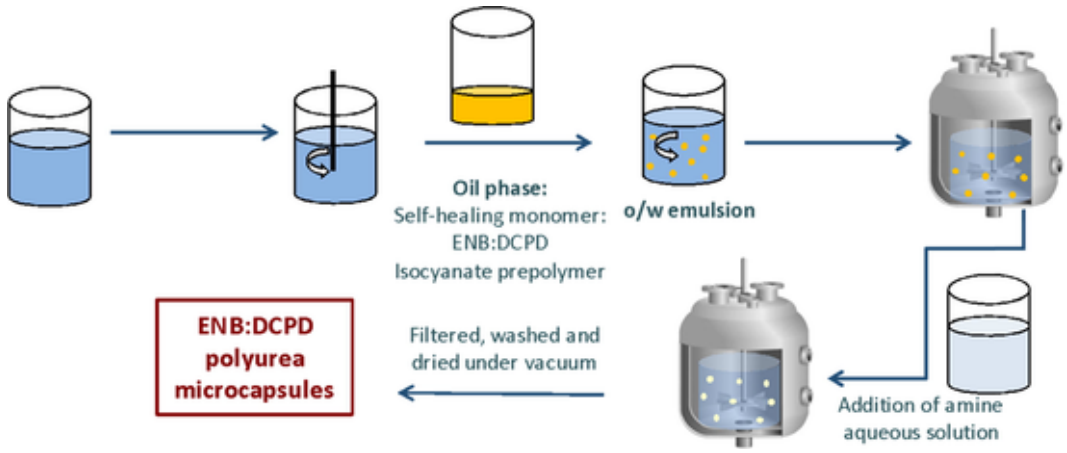

Fig. 2. Scheme of the protocol for ENB/CDPD microcapsules synthesis. (For interpretation of the references to colour in this figure legend, the reader is referred to the web version of this article.)

Table 4
. Summary of ENB/DCPD microencapsulation reaction conditions and results.

Entry	Emulsion step			Interfacial polymerization step						Core/shell ratio (Theorical)	MC size[a] (μm)	MC morphology	Degradation temperature[b] (°C)	Monomer content[b] (%)
	wt.% GA	Time (min)	Stirring (rpm)	Time (h)	Temperature (°C)	Stirring (rpm)	Amine	Amine:NCO ratio	Amine concentration (%)					
MC1	3	10	3000	1 + 1 + 1	r.t. + 50 + 70	300	EDA	1.1	1	70:30	21	Spherical	250	69
MC2	3	10	3000	1 + 1 + 1	r.t. + 50 + 70	300	DETA	1.1	1	70:30	34	Bulk material	–	–
MC3	3	10	3000	1 + 1 + 1	r.t. + 50 + 70	300	TETA	1.1	1	70:30	38	Bulk material	–	–
MC4	3	10	3000	1 + 1 + 1	r.t. + 50 + 70	300	EDA	1.1	1	60:40	41	Spherical (matrix)	237	25
MC5	3	10	3000	1 + 1 + 1	r.t. + 50 + 70	300	EDA	1.1	1	80:20	39	Spherical	217	69
MC6	3	10	3000	1 + 1 + 1	r.t. + 50 + 70	300	EDA	1.1	4	70:30	23	Spherical (matrix)	246	71
MC7	3	10	3000	1 + 1 + 1	r.t. + 50 + 70	300	EDA	1.1	10	70:30	25	Spherical (matrix)	–	–
MC8	3	10	3000	1 + 1 + 1	r.t. + 50 + 70	300	EDA	1.5	1	70:30	23	Spherical	250	54
MC9	3	10	3000	1 + 1 + 1	r.t. + 50 + 70	300	EDA	1.5	4	70:30	26	Spherical (matrix)	226	58
MC10	3	10	3000	1 + 1 + 1	r.t. + 50 + 70	300	EDA	1.5	10	70:30	25	Spherical (matrix)	–	–
MC11	3	10	3000	1 + 1 + 1	r.t. + 50 + 70	300	EDA	2	1	70:30	22	Spherical + elongated (mixture core/shell and matrix type)	–	–
MC12	3	10	3000	1 + 1 + 1	r.t. + 50 + 70	300	EDA	1.1	4	80:20	41	Elongated + artefacts	–	–
MC13	3	10	3000	1 + 1 + 1	r.t. + 50 + 70	300	EDA	1.1	4	90:10	39	Elongated + artefactsl	–	–
MC14	3	10	3000	1 + 1	r.t. + 50	300	EDA	1.1	1	70:30	21	Spherical	242	63
MC15	3	10	3000	3 h	70 °C	300	EDA	1.1	1	70:30	21	Spherical + artefacts	251	70
MC16	3	10	3000	4 h	70 °C	300	EDA	1.1	1	70:30	20	Spherical + artefacts	249	69
MC17	3	10	3000	o.n.	70 °C	300	EDA	1.1	1	70:30	20	Spherical + artefacts	244	67
MC18	3	10	5000	1 + 1 + 1	r.t. + 50 + 70	450	EDA	1.1	1	70:30	14	Spherical	246	56
MC19	3.5	20	5000	1 + 1 + 1	r.t. + 50 + 70	450	EDA	1.1	1	70:30	12	Spherical	246	70

[a] Median size determined in the Mastersizer 3000.
[b] Determined by TGA.

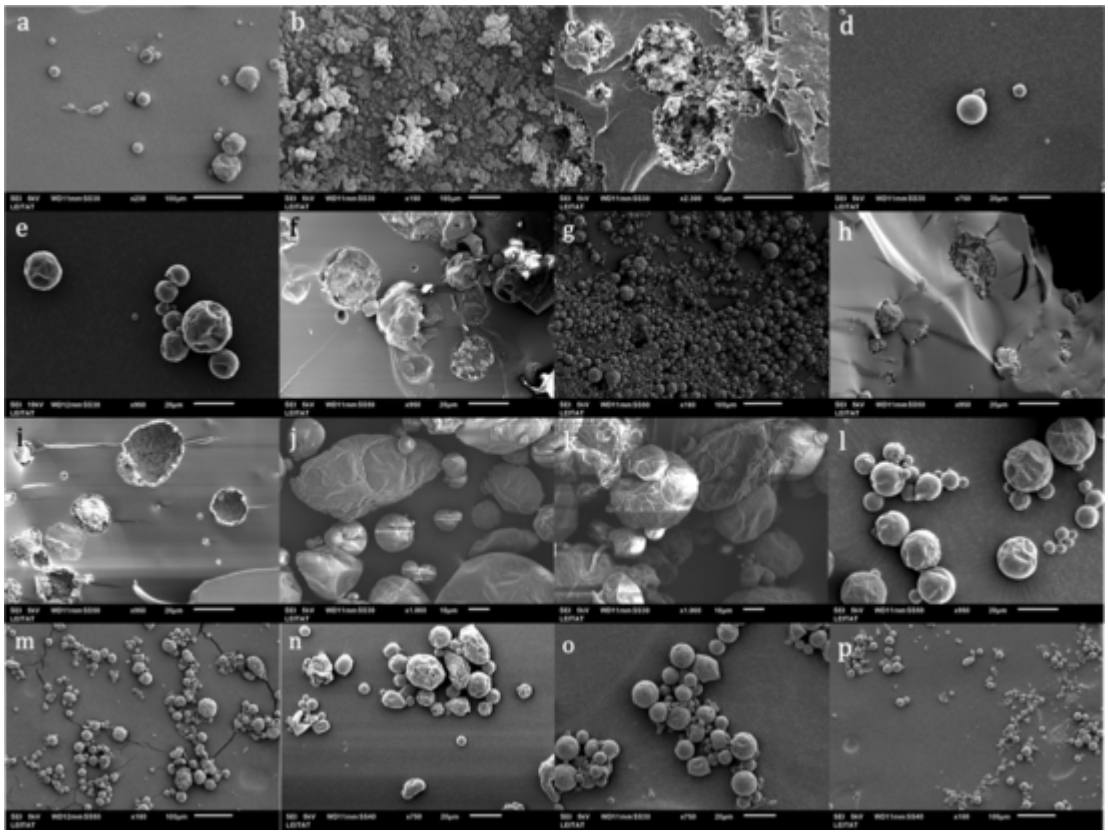

Fig. 3. SEM images of the different synthesized microcapsules. a- MC1; b-MC3; c-MC4; d-MC5; e-MC6; f-MC7; g-MC8; h-MC9; i-MC11; j-MC12; k-MC13; l-MC14; m-MC15; n-MC17; o-MC18 and p-MC19.

aqueous solution were studied in microcapsules with 70:30 core/shell fixed ratios (MC1 and MC6-MC11). The increase of amine equivalents produced materials with less load of encapsulated healing monomer and the free-isocyanate presence in the product was only slightly reduced (Fig. 4). The amine concentration did not show either a strong effect over isocyanate reactivity; furthermore, FESEM images of FIB crosscuts indicated that its increase led to microcapsules with a core-matrix structure instead of a core/shell structure. Within this observation, 1% EDA concentration with 1.1 amine equivalents to isocyanate were determined as best reactants system for polymerization.

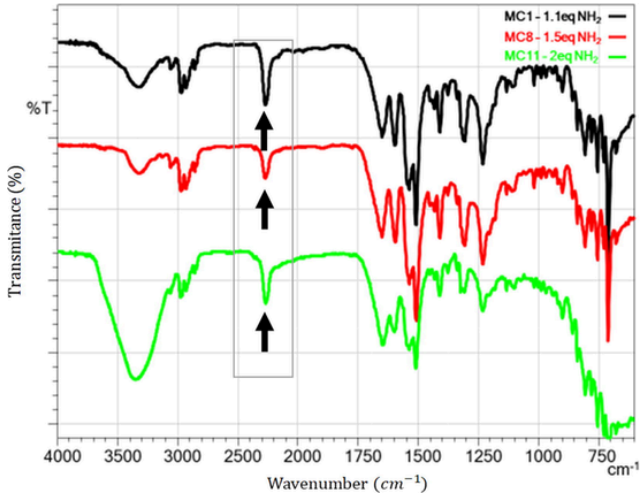

Fig. 4. FTIR spectra of the microcapsules produced by using 1.1 (black), 1.5 (red) and 2 (green) equivalents of ethylenediamine. The differences in isocyanate content produced by the modification of added equivalents can be observed at 2272 cm^{-1} as pointed by the arrows and the box. (For interpretation of the references to colour in this figure legend, the reader is referred to the web version of this article.)

Conversion of polyurea shell was further studied by the effect of reaction conditions: temperatures from room temperature to 70 °C and reaction times in a range of 2 h to overnight were applied (MC1 and MC14-MC17 microcapsules). Under milder conditions (MC1 and MC4), still a high quantity of free-isocyanate was detected by FTIR (Fig. 5). Reaction temperature and time were increased until non-free isocyanate was detected, what occurred at 70 °C and overnight reaction (Fig. 4), and thus full conversion was achieved. However, when the reaction was directly heated to 70 °C, the morphology of the capsules was more irregular when comparing to spherical morphologies obtained in mixtures initially stirred at 50 °C for 1 h (MC14), as depicted by the SEM micrographs (Fig. 3- l).

To better improve the encapsulation efficiency, the particle size distribution and shape of the microcapsules were optimized by modifying the parameters of the emulsion step (stirring rate and time), which is critical over these properties in interfacial encapsulation [45]. Accordingly, an increase in rotor speed during the emulsion step from 3000 to 5000 rpm (MC18) reduced the particle size (D_{50}) from 21 to 14 μm, despite the presence of some irregularities (Fig. 3- o) and lower healing content, 56%. The increase of emulsion stirring time from 10 to 20 min and the higher surfactant concentration, 3.5% gum Arabic (MC19) lead to core-shell spherical regular microcapsules (Fig. 3- p and Fig. 6 Top), with an encapsulation efficiency (relation between theoretical and measured monomer content) close to 100%. Although the modification of some parameters such as stirring velocity or emulsifier concentration and its effect on microcapsule morphology and size distribution are well known, its interesting to observe the effect of amine to isocyanate ratio and more importantly, amine concentration in the microcapsule core structure. As clearly depicted in Fig. 6, an increase of the amine concentration is the main factor producing the change from a matrix-

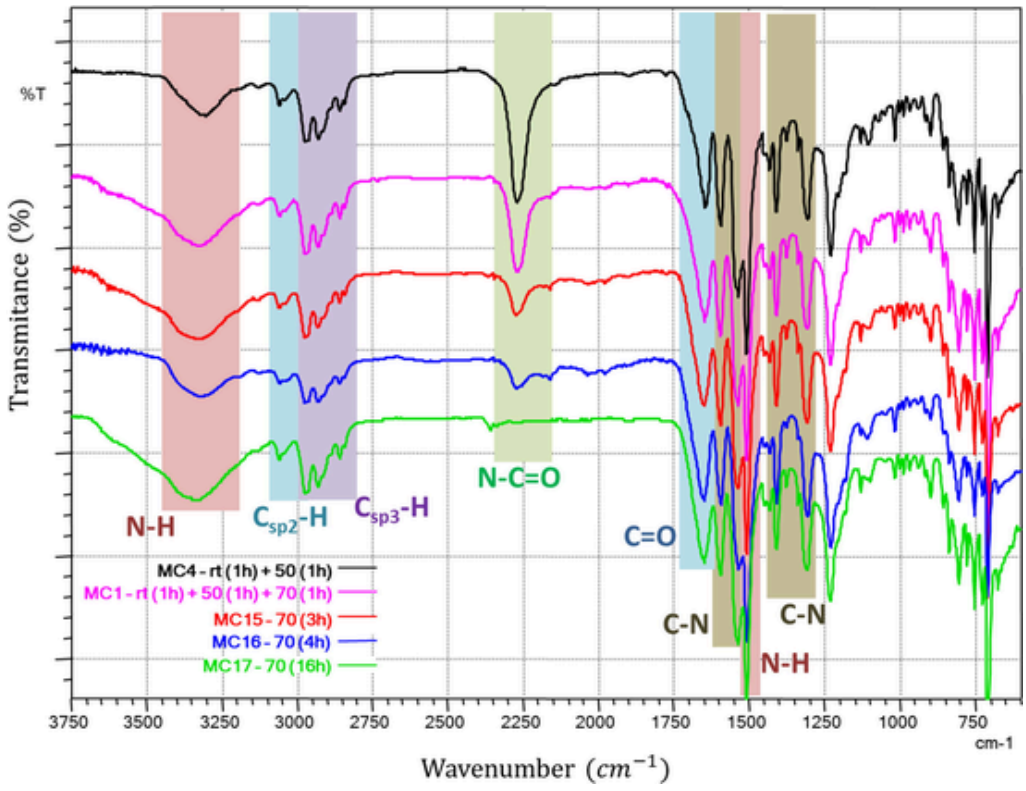

Fig. 5. Normalised FT-IR spectra of the encapsulation reaction at different temperatures and times. The differences in isocyanate content produced by the modification of procedure can be clearly observed at 2272 cm^{-1} as pointed by the decrease of the peak in comparison with the stable N-H signal at 1500 cm^{-1}. (For interpretation of the references to colour in this figure legend, the reader is referred to the web version of this article.)

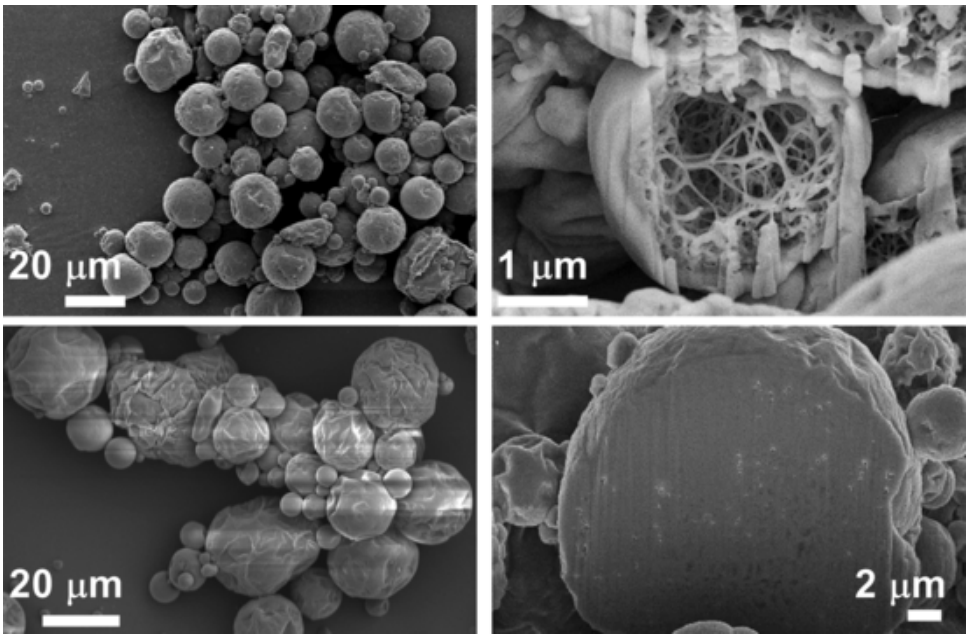

Fig. 6. SEM (left) and FIB-FESEM (right) micrographs of ENB/DCPD polyurea microcapsules synthesized employing TOP 1.1 eq of amine and 1 wt% of amine aqueous solution (Table 4, Entry MC19) and BOTTOM 1.5 eq of amine and 4 wt% of amine aqueous solution (Table 4, Entry MC9).

core type (Top) to an almost full-reacted sphere (Bottom), thus causing a huge decrease in the load capacity of the microvessel.

As physical-chemical characterization has demonstrated that MC19 microcapsules fulfilled desired proprieties, they were chosen for their incorporation in the epoxy resin.

3.3. Incorporation of ENB/DCPD microcapsules in epoxy resin

Achieving a homogeneous distribution of both SH capsules and ROMP catalyst is imperative to guarantee equal self-healing properties along the manufactured specimen. Moreover, SH additive homogeneity is necessary to increase the contact probability between the released content and curing agent after damage-induced breakage of the cap-

sules. Homogeneous distribution of both SH capsules and ROMP catalyst has been successfully achieved as it was observed by SEM micrographs of cured epoxy resin with 10 and 20 wt% (Supporting Information). Furthermore, the used concentration of SH additives is above the observed quantities for achieving a good reactivity thus, improving until almost a certain point the contact between monomer and catalyst in case of a crack.

Once an optimal distribution of the microcapsules over the resin was verified, as a mean to assess the process limitations, rheological studies of the instantaneous viscosity (mPa·s) on modified resins with different percentage of SH additives were performed prior to specimen manufacturing. Loads of 10, 20 and 30 wt% of SH capsules were compared to the neat resin. Epoxy resin systems Epikote 135-Epikure 137 and Araldite LY556-Aradur 917 were chosen as references due to their posterior use in industrial infusion process, in which viscosities above 2000 mPa·s are not viable. For this reason, 2000 mPa·s was stablished as the limit-line.

From the rheological studies, we can determine that the viscous behaviour of the neat resin displays a non-Newtonian pattern, more specifically a shear-thinning tendency where the instantaneous viscosity decreases as the shear velocity increases. The same pattern is followed yet enhanced as more SH additives are introduced into the epoxy component. This effect is seen is both resins but more intensely in the Epikote-Epicure system.

In both studied systems, only loads of 10 wt% always fulfil the viscosity requirements for the final applications, becoming thus the optimal load for production processes with both epoxy systems in terms of achieving the highest possible load of SH additives while maintaining the potential industrial processability. However, upon certain shear, both epoxy systems loaded with 20 wt% of MCs, displays values below the limit-line of viscosity. Thus, certain adaptations will allow higher loads if higher self-healing additives charge is needed.

Viscosity of CTD 7.1 epoxy system was not critical as the composite manufacture did not present the previous limitation. However, 10 wt% of SH microcapsule loading was also used for this system with the aim of having the same quantity of self-healing additives among samples under study.

3.4. SH efficiency assessed by fracture test results

Once the SH additive load was stablished at 10 wt% results of fracture TDCB specimens with and without microcapsules were compared and the self-healing efficiency was determined.

Initially, due to material shortage, the focus of study was limited to only neat and SH modified Epikote 135/137 epoxy resin specimens. Specimens containing 10 wt% of SH additives were tested for the epoxy resin system, along with another neat epoxy resin samples used as reference. Samples of both kind of specimens were manufactured with the optimal geometry for fracture SH studies [38,40,46]. Tests evaluating the SH efficiency at cryogenic temperatures with both modified and unmodified resins were evaluated per triplicate and the results are summarized in Table 4. While neat specimens exhibited a fracture force near 190 N, there is a reduction to 133 N when self-healing additives are included into the epoxy resin. Unlike other researchers reported [47], SH additives produced a decrease on the fracture toughness values of the specimens. In this sense, other parameters including microcapsule size, shell composition, aggregation effects and G3 catalyst interaction with the resin could be held responsible for such effect. Further and deeper research would be needed for this hypothesis verification.

The SH efficiency (η_{SH}) was calculated by means of Eq. (2), using the obtained critical fracture load of both virgin and healed sample at low/ultra-low temperatures. Regardless of initial decrease in values, fracture healing tests in SH modified Epikote 135 epoxy resin exhibited η_{SH} values of 115% at low/ultra-low temperatures.

Accounting for the excellent SH capacity obtained for the first epoxy system, one SH modified specimen of Araldite LY556 and one of CTD7.1 epoxy systems were manufactured in order to observe if these results could be extrapolated into other epoxy resin systems. SH fracture toughness results for those systems are summarized in Table 5.

According to the load-displacement curves (Fig. 7), differences between fracture forces of specimens with and without SH followed the same behaviour of the first studied system, where additives appear to have caused a slight decrease in the toughness of the specimens. Similarly to Epikote modified resin, both Araldite and CTD 7.1 SH specimens demonstrated SH capacity with efficiencies of 116% and 133% respectively at low temperatures leading thusto a tougher material after healing in all studied systems, while no effect was observed in reference specimens. This demonstrates the versatility of the SH systems efficiency for different epoxy resins at cryogenic conditions. The observed trend is in good agreement with those reported in previous studies [19,26].

The authors acknowledge the simplistic yet most common approach for the self-healing studies that the TDCB provide in regard to other techniques studying the damage on continuum mechanics [18] that can be more representative but appears to have a higher degree in complexity that falls out of the current scope of this work.

3.5. Fracture surface morphology.

Several fracture surfaces of different SH specimens were analyzed by SEM microscopy after conducting the fracture tests (Fig. 8). Comparing the fractured surface of the healed samples after performing the SH test to those observed in areas of the modified specimens that were not damaged, the surface morphology and microstructure are completely different in terms of surface roughness. This phenomena is produced due to the lack of observable microcapsules in the fractured region of the self-healed specimens (Fig. 8b). These observations could imply that, during the fracture test, the microcapsules broke and their content effectively interacted with the catalyst, repairing the induced microcracks and thus, performing the desired and observed SH effect shown in Fig. 7, whereas in the rest of the specimen, no damage was induced and therefore, the SH microcapsules remain intact (Fig. 8a). Moreover, the hypothesized specimen embrittlement due to the microcapsules addition, can be attributed to the observed, intact and marked microsphere clusters (yellow highlighted square in Fig. 8a). These aggregates, although having a scarce presence in the resin as observed by SEM (SI), may be generating secondary phases and non-coherent interfaces that in turn, could potentially be the reason for the decrease of toughness of the SH modified specimens in comparison with the neat ones. Additionally, a closer inspection of a region of a tested modified specimen, exhibit the reacted SH microcapsules completely integrated in the matrix as well as a bad adhesion between the microcapsules and the resin employed in a non-damaged area of the specimens (Fig. 8c). These results contribute to the hypothesis that the self-healing additives are the main drivers for the samples embrittlement as well as confirm

Table 5
Epikote, Araldite and CTD epoxy systems Self-Healing results.

Resin	Virgin (N)	Healed (N)	% healing[a]
Epikote 135/Epikure 137 – 10% Self-Healing additives	133.3 ± 18.9	153.2 ± 24.9	114.8 ± 9.1
Epikote 135/Epikure 137	187.1 ± 12.3	25.3 ± 3.0	–
Araldite LY556/Aradur 917 – 10% SHMC	109.5	127.3	116
Araldite LY556/Aradur 917	132.5 ± 7.4	17.0 ± 2.0	–
CTD 7.1 – 10% SHMC	100	134	134
CTD 7.1	150.5 ± 16.1	20.0 ± 3.3	–

[a] 100% of self-healing efficiency was considered when the healed sample demonstrates the same level of critical fracture load than the virgin one.

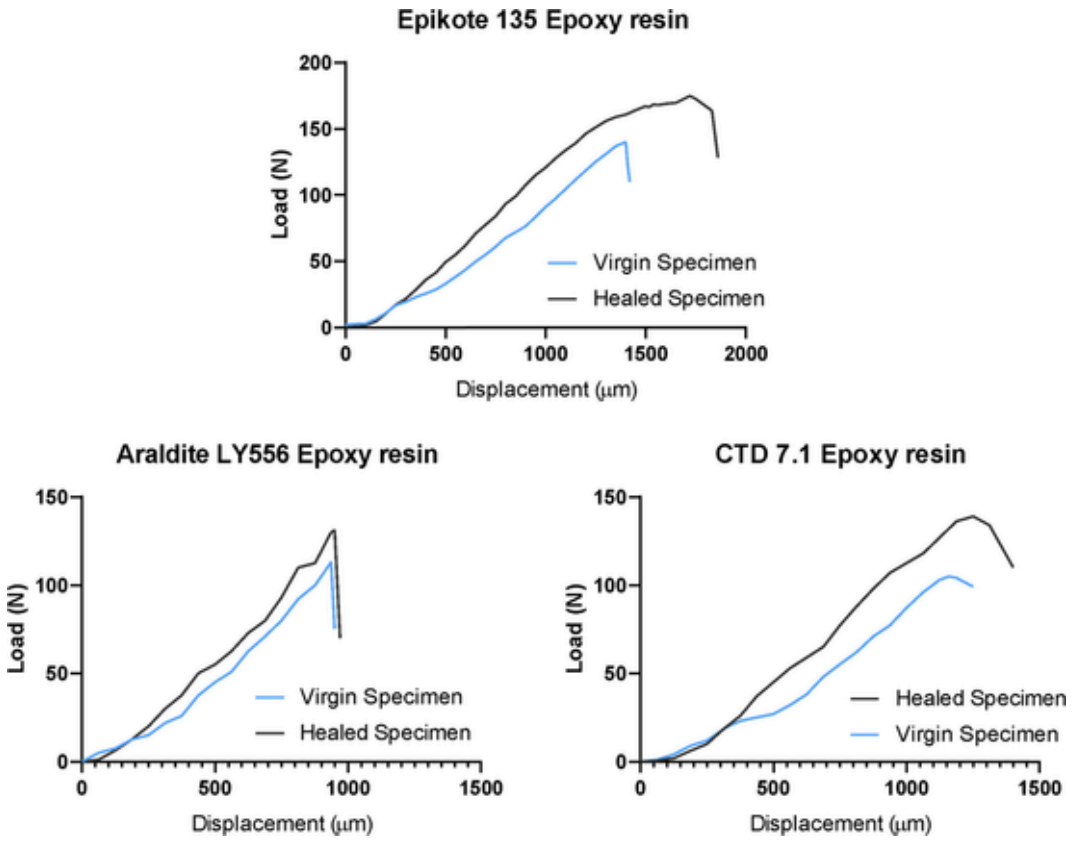

Fig. 7. Representative force vs displacement curves of epoxy resins manufactured with ENB/DCPD microparticles. Higher values of fracture toughness are observed in the three epoxy systems after the healing process. (For interpretation of the references to colour in this figure legend, the reader is referred to the web version of this article.)

the release and reaction of the self-healing monomers at the studied temperatures. Even though the introduction of these SH system could appear to slightly compromise the epoxy material toughness, it should not affect significantly the final composite mechanical properties when the Carbon or Glass fibre reinforcement is added. Moreover, the possible presence of small clusters inside the composite did not compromise the healing effect as shown in Fig. 7 as randomized samples from the same batch were used both for the SH testing and the surface characterization.

4. Conclusions

In this work, the comprehensive study was successfully performed regarding fluidity and chemical reactivity of different ENB/DCPD mixtures, catalysts type (HG2, G3) and concentration (0.1–0.004%). It has been proven that the system can flow and fill the crack at ultra-low temperatures (−70 °C) and react with G3 catalyst promoting the ROMP reaction at cryogenic temperatures (−20 °C) facing composite real applications. The microencapsulation of the ENB/DCPD mixture in pMDI-based polyurea by interfacial polymerization allowed a wide range of core-shell materials with high healing agent load.

A load of 10 wt% of SH additives was proven optimal to maintain the viscosity values within the working range given by large-scale manufacturing processes. Extrinsic self-healing system based on ENB/DCPD blend and G3 catalyst did not affect the epoxy system curing process.

The use of TDCB geometry helped in understanding the crack propagation and the fracture properties of microcapsules reinforced epoxy composites.

The developed system demonstrated self-healing values up to 134% at low and ultra-low temperatures. Crack surface morphology images obtained by SEM before and after the self-healing process confirmed the feasibility of the breaking and curing mechanism of the extrinsic system.

Even though most of the research exhibited in this work has been done in different systems of epoxy materials, both the additives size and its concentration have been optimized for an industrial scale-up and application for FRP manufacture.

As a summary, we have developed an autonomous, extrinsic self-healing system that has demonstrated flowability at ultra-low temperatures (−70 °C) and a highly efficient automatic repair at cryogenic temperatures (−20 °C) without the need of catalyst protection in three different commercial epoxy resins traditionally used in fields as automotive, aeronautics and wind energy. Moreover, due to the excellent results derived from this work, little modifications can be generated to adapt the system to a broad range of polymeric materials and therefore, to an extremely wide field of applications.

Declaration of Competing Interest

The authors declare that they have no known competing financial interests or personal relationships that could have appeared to influence the work reported in this paper.

Acknowledgments

We thank Dr. Lorenzo Bautista and Hector Linuesa for useful discussions. We thank Dr. Pau Nolis (Universitat Autònoma de Barcelona) for his technical assistance in NMR spectroscopy. We thank Quimidroga S.A. for providing Voranate™ M 2940. This work has received funding from the European Union's Horizon 2020 research and innovation programme under grant agreement No 685842. J.J. Roa acknowledges the

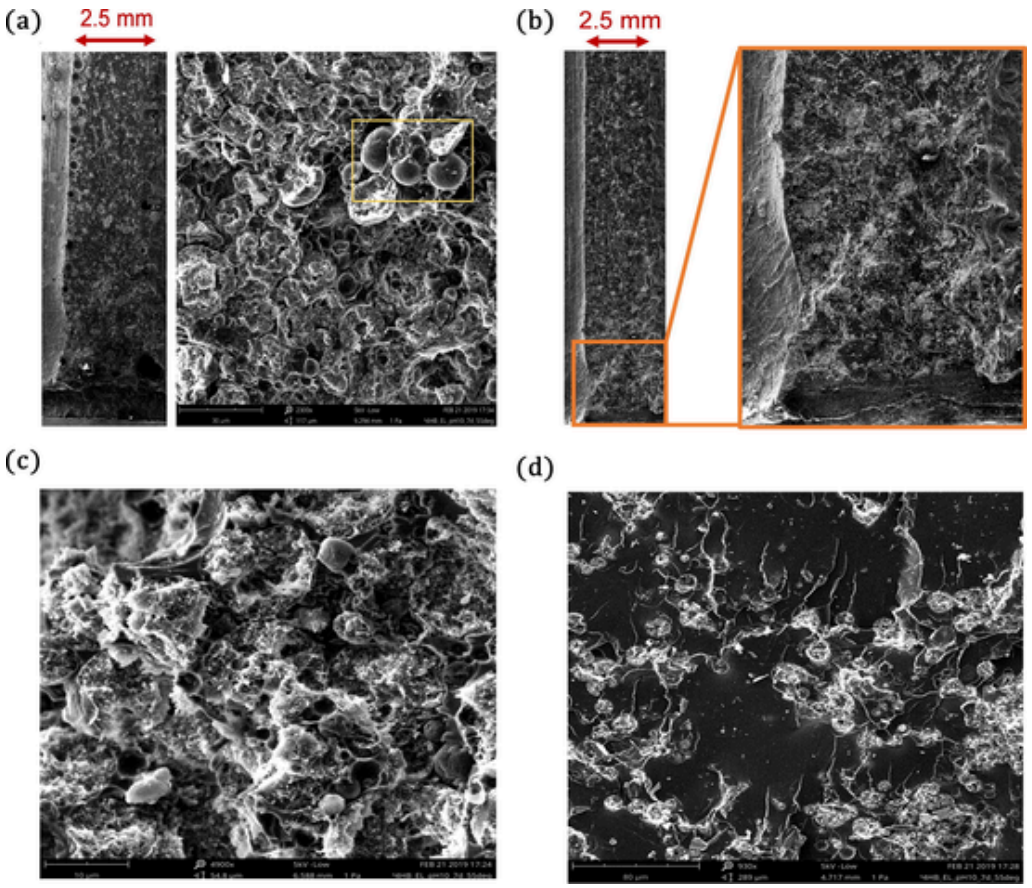

Fig. 8. TOP- SEM micrographs of the Epikote 135 epoxy composites with SH additives. (a) non-damaged area where the capsules can be seen intact on the yellow square and (b) self-healed specimen where the surface of the specimen does not show any apparent microcapsule due to the SH effect. BOTTOM - SEM micrographs from a tested modified specimen. (c) In the fracture region, where it can be appreciated a reacted core of the microcapsules and its surroundings and (d) far from the fracture zone. (For interpretation of the references to colour in this figure legend, the reader is referred to the web version of this article.)

Serra Hunter programme of the Generalitat de Catalunya. This work has also been done in the framework of the doctorate in Material Sciences of the Autonomous University of Barcelona.

Appendix A. Supplementary data

Supplementary data to this article can be found online at https://doi.org/10.1016/j.compositesa.2021.106335.

References:

[1] Mugahed Amran YH, Alyousef R, Rashid RSM, Alabduljabbar H, Hung C-C Properties and applications of FRP in strengthening RC structures: a review. Structures 2018;16:208–38. https://doi.org/10.1016/j.istruc.2018.09.008.
[2] Hopmann C, Ophüls M, Hildebrandt M, Fischer K Flexible production of thermoset FRP components. Lightweight Des Worldw 2018;11:54–9. https://doi.org/10.1007/s41777-018-0027-7.
[3] Patnaik A, Satapathy A, Chand N, Barkoula NM, Biswas S Solid particle erosion wear characteristics of fiber and particulate filled polymer composites: a review. Wear 2010;268:249–63. https://doi.org/10.1016/j.wear.2009.07.021.
[4] Vigneshwaran S, Uthayakumar M, Arumugaprabu V A review on erosion studies of fiber-reinforced polymer composites. J Reinf Plast Compos 2017;36:1019–27. https://doi.org/10.1177/0731684417699711.
[5] Mohan N, Mahesha CR, Rajaprakash BM Erosive wear behaviour of WC filled glass epoxy composites. Procedia Eng 2013;68:694–702. https://doi.org/10.1016/j.proeng.2013.12.241.
[6] Yang Y, Urban MW Self-healing polymeric materials. Chem Soc Rev 2013;42:7446. https://doi.org/10.1039/c3cs60109a.
[7] Leeuwenburgh SCG, De Belie N, van der Zwaag S Self-healing materials are coming of age. Adv Mater Interfaces 2018;5:1800736. https://doi.org/10.1002/admi.201800736.
[8] Dahlke J, Zechel S, Hager MD, Schubert US How to design a self-healing polymer: general concepts of dynamic covalent bonds and their application for intrinsic healable materials. Adv Mater Interfaces 2018;5:1800051. https://doi.org/10.1002/admi.201800051.
[9] Zhong N, Post W Self-repair of structural and functional composites with intrinsically self-healing polymer matrices: a review. Compos Part Appl Sci Manuf 2015;69:226–39. https://doi.org/10.1016/j.compositesa.2014.11.028.
[10] Ullah H, M Azizli KA, Man ZB, Ismail MBC, Khan MI. The Potential of Microencapsulated Self-healing Materials for Microcracks Recovery in Self-healing Composite Systems: A Review. Polym Rev 2016;56:429–85. https://doi.org/10.1080/15583724.2015.1107098.
[11] An S, Lee MW, Yarin AL, Yoon SS A review on corrosion-protective extrinsic self-healing: comparison of microcapsule-based systems and those based on core-shell vascular networks. Chem Eng J 2018;344:206–20. https://doi.org/10.1016/j.cej.2018.03.040.
[12] Wang S, Urban MW Self-healing polymers. Nat Rev Mater 2020;5:562–83. https://doi.org/10.1038/s41578-020-0202-4.
[13] Hu Z, Zhang D, Lu F, Yuan W, Xu X, Zhang Q, et al. Multistimuli-responsive intrinsic self-healing epoxy resin constructed by host-guest interactions. Macromolecules 2018;51:5294–303. https://doi.org/10.1021/acs.macromol.8b01124.
[14] Kim D-M, Cho Y-J, Choi J-Y, Kim B-J, Jin S-W, Chung C-M Low-temperature self-healing of a microcapsule-type protective coating. Materials 2017;10:1079. https://doi.org/10.3390/ma10091079.
[15] Hu Z, Liu Y, Xu X, Yuan W, Yang L, Shao Q, et al. Efficient intrinsic self-healing epoxy acrylate formed from host-guest chemistry. Polymer 2019;164:79–85. https://doi.org/10.1016/j.polymer.2019.01.010.
[16] Kumar Banshiwal J, Nath Tripathi D. Self-Healing Polymer Composites for Structural Application. In: Sahu D, editor. Funct. Mater., IntechOpen; 2019. https://doi.org/10.5772/intechopen.82420.
[17] Cohades A, Branfoot C, Rae S, Bond I, Michaud V Progress in self-healing fiber-reinforced polymer composites. Adv Mater Interfaces 2018;5:1800177. https://doi.org/10.1002/admi.201800177.
[18] Tan PS, Somashekar AA, Casari P, Bhattacharyya D Healing efficiency characterization of self-repairing polymer composites based on damage continuum mechanics. Compos Struct 2019;208:367–76. https://doi.org/10.1016/j.compstruct.2018.09.091.

[19] White SR, Sottos NR, Geubelle PH, Moore JS, Kessler MR, Sriram SR, et al. Autonomic healing of polymer composites. Nature 2001;409:794–7. https://doi.org/10.1038/35057232.
[20] Rule JD, Brown EN, Sottos NR, White SR, Moore JS Wax-protected catalyst microspheres for efficient self-healing materials. Adv Mater 2005;17:205–8. https://doi.org/10.1002/adma.200400607.
[21] Forcina V, García-Domínguez A, Lloyd-Jones GC Kinetics of initiation of the third generation Grubbs metathesis catalyst: convergent associative and dissociative pathways. Faraday Discuss 2019;220:179–95. https://doi.org/10.1039/C9FD00043G.
[22] Brown EN, Kessler MR, Sottos NR, White SR In situ poly(urea-formaldehyde) microencapsulation of dicyclopentadiene. J Microencapsul 2003;20:719–30. https://doi.org/10.1080/0265204031000154160.
[23] Lee JK, Hong SJ, Liu X, Yoon SH Characterization of dicyclopentadiene and 5-ethylidene-2-norbornene as self-healing agents for polymer composite and its microcapsules. Macromol Res 2004;12:478–83. https://doi.org/10.1007/BF03218430.
[24] Noh HH, Lee JK Microencapsulation of self-healing agents containing a fluorescent dye. Express Polym Lett 2013;7:88–94. https://doi.org/10.3144/expresspolymlett.2013.8.
[25] Urdl K, Kandelbauer A, Kern W, Müller U, Thebault M, Zikulnig-Rusch E Self-healing of densely crosslinked thermoset polymers—a critical review. Prog Org Coat 2017;104:232–49. https://doi.org/10.1016/j.porgcoat.2016.11.010.
[26] Raimondo M, Longo P, Mariconda A, Guadagno L Healing agent for the activation of self-healing function at low temperature. Adv Compos Mater 2015;24:519–29. https://doi.org/10.1080/09243046.2014.937135.
[27] Kalista SJ, Pflug JR, Varley RJ Effect of ionic content on ballistic self-healing in EMAA copolymers and ionomers. Polym Chem 2013;4:4910. https://doi.org/10.1039/c3py00095h.
[28] Tiwari N, Ho F, Ankit A, Mathews N A rapid low temperature self-healable polymeric composite for flexible electronic devices. J Mater Chem A 2018;6:21428–34. https://doi.org/10.1039/C8TA08328B.
[29] Ying H, Zhang Y, Cheng J Dynamic urea bond for the design of reversible and self-healing polymers. Nat Commun 2014;5:3218. https://doi.org/10.1038/ncomms4218.
[30] Wu X, Luo R, Li Z, Wang J, Yang S Readily self-healing polymers at subzero temperature enabled by dual cooperative crosslink strategy for smart paint. Chem Eng J 2020;398:125593. https://doi.org/10.1016/j.cej.2020.125593.
[31] Xue S, Wu Y, Guo M, Xia Y, Liu D, Zhou H, et al. Self-healable poly(acrylic acid- *co* -maleic acid)/glycerol/boron nitride nanosheet composite hydrogels at low temperature with enhanced mechanical properties and water retention. Soft Matter 2019;15:3680–8. https://doi.org/10.1039/C9SM00179D.
[32] Nevejans S, Ballard N, Fernández M, Reck B, García SJ, Asua JM The challenges of obtaining mechanical strength in self-healing polymers containing dynamic covalent bonds. Polymer 2019;179:121670. https://doi.org/10.1016/j.polymer.2019.121670.
[33] Brown EN Use of the tapered double-cantilever beam geometry for fracture toughness measurements and its application to the quantification of self-healing. J Strain Anal Eng Des 2011;46:167–86. https://doi.org/10.1177/0309324710396018.
[34] Sutthasupa S, Shiotsuki M, Sanda F Recent advances in ring-opening metathesis polymerization, and application to synthesis of functional materials. Polym J 2010;42:905–15. https://doi.org/10.1038/pj.2010.94.
[35] Specht S, Bluhm J, Schröder J. Continuum Mechanical Description of an Extrinsic and Autonomous Self-Healing Material Based on the Theory of Porous Media. In: Hager MD, van der Zwaag S, Schubert US, editors. Self-Heal. Mater., vol. 273, Cham: Springer International Publishing; 2015, p. 143–84. https://doi.org/10.1007/12_2015_338.
[36] Song K, Kim K, Hong D, Kim J, Heo CE, Kim HI, et al. Highly active ruthenium metathesis catalysts enabling ring-opening metathesis polymerization of cyclopentadiene at low temperatures. Nat Commun 2019;10:3860. https://doi.org/10.1038/s41467-019-11806-5.
[37] Li Q, Siddaramaiah KNH, Hui D, Lee JH Effects of dual component microcapsules of resin and curing agent on the self-healing efficiency of epoxy. Compos Part B Eng 2013;55:79–85.. https://doi.org/10.1016/j.compositesb.2013.06.006.
[38] Petersen D, Link R, Beres W, Koul A, Thamburaj R A tapered double-cantilever-beam specimen designed for constant-K testing at elevated temperatures. J Test Eval 1997;25:536. https://doi.org/10.1520/JTE11493J.
[39] Kanu NJ, Gupta E, Vates UK, Singh GK Self-healing composites: a state-of-the-art review. Compos Part Appl Sci Manuf 2019;121:474–86. https://doi.org/10.1016/j.compositesa.2019.04.012.
[40] Garoz Gómez D, Gilabert FA, Tsangouri E, Van Hemelrijck D, Hillewaere XKD, Du Prez FE, et al. In-depth numerical analysis of the TDCB specimen for characterization of self-healing polymers. Int J Solids Struct 2015;64–65:145–54. https://doi.org/10.1016/j.ijsolstr.2015.03.020.
[41] Sheng X, Lee JK, Kessler MR Influence of cross-link density on the properties of ROMP thermosets. Polymer 2009;50:1264–9. https://doi.org/10.1016/j.polymer.2009.01.021.
[42] Yang G, Mauldin TC, Lee JK Cure kinetics and physical properties of poly(dicyclopentadiene/5-ethylidene-2-norbornene) initiated by different Grubbs' catalysts. RSC Adv 2015;5:59120–30. https://doi.org/10.1039/C5RA05335H.
[43] Leitgeb A, Wappel J, Slugovc C The ROMP toolbox upgraded. Polymer 2010;51:2927–46. https://doi.org/10.1016/j.polymer.2010.05.002.
[44] Huang M, Yang J Facile microencapsulation of HDI for self-healing anticorrosion coatings. J Mater Chem 2011;21:11123. https://doi.org/10.1039/c1jm10794a.
[45] Salaün F, Bedek G, Devaux E, Dupont D, Gengembre L Microencapsulation of a cooling agent by interfacial polymerization: Influence of the parameters of encapsulation on poly(urethane–urea) microparticles characteristics. J Membr Sci 2011;370:23–33. https://doi.org/10.1016/j.memsci.2010.11.033.
[46] Guadagno L, Vertuccio L, Naddeo C, Calabrese E, Barra G, Raimondo M, et al. Self-healing epoxy nanocomposites via reversible hydrogen bonding. Compos Part B Eng 2019;157:1–13. https://doi.org/10.1016/j.compositesb.2018.08.082.
[47] Li H, Wang R, Liu W Toughening self-healing epoxy resin by addition of microcapsules. Polym Polym Compos 2011;19:223–6. https://doi.org/10.1177/0967391111019002-326.